Draft version March 6, 2022
Typeset using LaTeX twocolumn style in AASTeX631

SN 2020jgb

Authors[1]

[1] Center for Interdisciplinary Exploration and Research in Astrophysics (CIERA), Department of Physics and Astronomy, Northwestern University, 2145 Sheridan Road, Evanston, IL 60208, USA

ABSTRACT

Keywords: keywords

1. INTRODUCTION

- SN 2016jhr (Jiang et al. 2017)
- SN 2016hnk as a He-shell double detonation (Jacobson-Galán et al. 2020); as a near-Chandrasekhar mass, 91bg-like object (Galbany et al. 2019)
- SN 2018byg (De et al. 2019)
- SN 2019ofm (De et al. 2020)

2. OBSERVATIONS

2.1. *Detection and Classification*

SN 2020jgb was first discovered by the Zwicky Transient Facility (ZTF; Bellm et al. 2019; Graham et al. 2019) on 2020 May 03.463 UT (MJD 58972.463) with the 48-inch Samuel Oschin Telescope (P48) at Palomar Observatory. The internal designation is ZTF20aayhacx. It was detected at a magnitude of 19.86 in ZTF g-band, and J2000 coordinates $\alpha = 17^{\rm h}53^{\rm m}12^{\rm s}.651$, $\delta = -00^\circ51'21''.81$. The last non-detection was on 2020 April 27.477 (MJD 58966.477; 5.99 days before the first detection) up to a limiting magnitude of 20.7 in ZTF r-band.

Classification, ...

2.2. *Optical Photometry*

We obtained gr-band photometry of SN 2020jgb with the ZTF camera. A Galactic extinction of $E(B-V) = 0.404$ is reported by the maps of Schlafly & Finkbeiner (2011), for which we correct all our photometry using the extinction model proposed by Fitzpatrick (1999). We do not account for any additional host extinction due to the lack of any Na I D absorption in our spectra.

2.3. *Optical Spectroscopy*

Table 1. Spectroscopic Observations of SN 2020jgb

$t_{\rm obs}$ (MJD)	Phase (d)	Telescope/ Instrument	R ($\Delta\lambda/\lambda$)	Range (Å)	Air Mass
58,976.42	−9.7	P60/SEDM	100	3770–9220	1.23
58,982.12	−4.2	NOT/ALFOSC	360	4000–9620	1.17
58,990.43	+3.9	P60/SEDM	100	3770–9220	1.23
58,997.44	+10.7	P60/SEDM	100	3770–9220	1.29
58,998.00?	+11.2?	Shane/Kast	500?	3620–10720	
59,008.41	+21.3	P60/SEDM	100	3770–9220	1.28
59,010.00?	+22.9?	P200/DBSP	700	3200–9500	
59,023.58	+36.1	Keck I/LRIS	1100	3200–10250	2.04
59,107.29	+117.3	Keck I/LRIS	1100	3200–10250	1.31
59,143.26	+152.2	Keck I/LRIS	1100	3200–10250	2.16

Note—Phase is measured relative to $t_{r,\rm peak}$ in the host galaxy rest frame. The resolution R is reported for the central region of the spectrum.

We obtained optical spectroscopic follow-up of the object from ≈ -10 days to $\approx +150$ days after the r-band peak, using the Spectral Energy Distribution Machine (SEDM; Blagorodnova et al. 2018) on the automated 60 inch telescope (P60; Cenko et al. 2006) at Palomar Observatory, the Kast Double Spectrograph[1] at the Shane 3 m Telescope, the Andalucia Faint Object Spectrograph and Camera (ALFOSC)[2] installed at the Nordic Optical Telescope (NOT), the Double Beam Spectrograph (DBSP) on the 200 inch Hale telescope (P200; Oke & Gunn 1982), the Low Resolution Imaging Spectrograph (LRIS) on the Keck I telescope (Oke et al. 1995).

2.4. *Near-infrared (NIR) Spectroscopy*

We obtained one NIR (0.8-2.5 μm) spectrum of the transient using the Gemini near-infrared spectrometer

[1] https://mthamilton.ucolick.org/techdocs/instruments/kast/

[2] https://www.not.iac.es/instruments/alfosc/

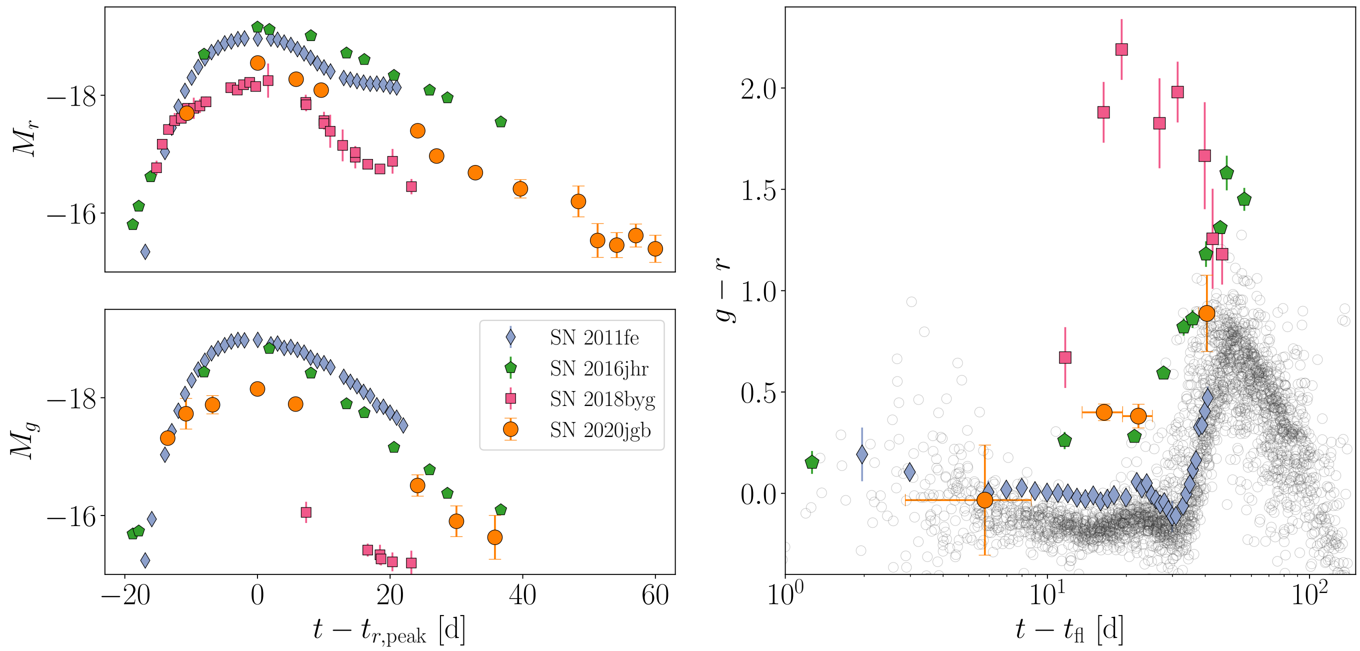

Figure 1. *Left*: comparison of the multi-color (g and r bands) light curves of SN 2020jgb to the normal SN Ia SN 2011fe and the He double detonation candidate SN 2018byg. *Right*: comparison of $g-r$ color evolution to SN 2011fe and SN 2018byg, as well as 62 normal SNe Ia (open circles) with prompt observations within 5 days of first light by ZTF (Bulla et al. 2020). The shaded region denotes the 1-σ credible interval of the color of SN 2020jgb until ≈40 days after the peak, estimated using Gaussian process.

(GNIRS; Elias et al. 1998) on the Gemini North telescope on 2020 June 9 (≈22 days after r-band peak), for an integration time of 2400 s. The spectra were reduced with the `PypeIt` Python package (Prochaska et al. 2020; Prochaska et al. 2020).

3. ANALYSIS

3.1. *Photometric Properties*

- sub-luminous
- first light time, peak time
- color evolution

3.2. *Spectroscopic Properties*

- infrared Ca II triplet (Ca II IRT)
- tentative He I absorption at ≈1 μm

3.3. *NIR spectra*

In Figure 3, the NIR spectrum is presented along with three spectra in the sample of Marion et al. (2009) at similar phases. SN 2020jgb shows a strong absorption feature at ≈0.99 μm, which is not seen in normal SNe Ia. This feature was still significant two weeks later, as detected by LRIS on Keck (see Figure 4), though it was only partially covered due to the limitation of bandwidth. In general, SN 2020jgb highly resembles normal SNe Ia in NIR band. The shape of the continuum redwards to ≈1.2 μm is significantly altered by line-blanketing of Fe-group elements synthesized in the SN interior, as opposed to the Fe-group elements in the outermost region as ashes of shell helium burning. Just like normal SNe Ia, SN 2020jgb also show enhancement of flux at about 1.3, 1.55, 2.0, 2.1, and 2.25 μm, accompanied by several Co II absorption lines. It is especially similar to SN 2004da at +25 days after maximum as the steep increase in flux at ≈1.55 μm, known as the H-band break, has become less prominent.

What is not seen in usual SNe Ia is the wide, deep absorption at ≈0.99 μm (hereafter the 1 μm feature), indicating its peculiarity. According to Marion et al. (2009), normal SNe Ia are nearly featureless in spectra around 1 μm a few weeks past the week. There are several elements that may be associated with this feature. None of these identifications is fully satisfying, and usually other strong lines of the same elements are missing in the spectra. The nature of the 1 μm feature remains uncertain. Chances are that this absorption is a mixture of multiple weaker lines.

The most attractive possibility is the strong He I line at 1.0830 μm, as has predicted in sub-Chandrasekhar-mass He-shell double detonation models when consider-

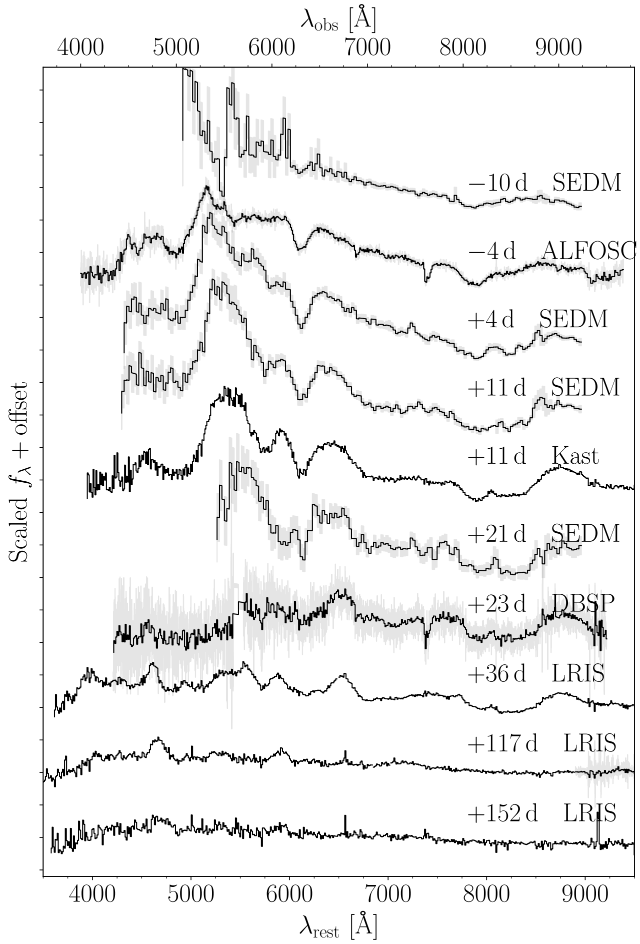

Figure 2. Optical spectroscopic sequence of SN 2020jgb. Rest frame phases (days) relative to the r-band peak and instruments used are posted next to each spectrum. The black curves are binned spectra with a bin size of 10 Å, except for the SEDm spectra, whose resolution is lower. The 1-σ uncertainties of raw spectra are shown in grey. Only regions with SNR > 3 after binning are plotted.

able amount of helium in the shell is left unburnt (Boyle et al. 2017). Figure 4 shows that the 1 μm feature, if associated with He I λ1.0830 μm, has a high velocity (≈26,000 km/s), yet similar as the HVF of Ca II IRT (≈24,000 km/s). The expansion velocity in the ejecta is roughly linearly proportional to the radius, so such a high velocity indicates that both the Ca II IRT and the tentative He I absorption line form far outside the normal photosphere, which has a velocity of only ≈10,000 km/s. In the sense, the He-shell double detonation scenario, in which the unburnt helium locates at the outermost ejecta, is indeed supported.

Still, this helium detection remains skeptical, since other He I are not unambiguously detected, such as the He I λ2.0581 μm. Considering a line velocity of ≈26,000 km/s and a host galaxy redshift of 0.0307, this line will be blueshifted to ≈1.95 μm in the observer frame, so will be strongly blended by the strong telluric lines within 1.8-2.0 μm. After telluric correction, the signal to noise ratio reaches ∼5, with which we still cannot see any significant absorption feature. An upper limit of the equivalent width is determined to be < 2% of the 1.0830 μm line, while theoretically, the 2.0581 μm line is supposed to be only a factor of 6-12 weaker, depending on temperature (Marion et al. 2009). Another fact is that the 1 μm feature is as strong as the He I λ1.0830 μm in many helium-rich core-collapse supernovae, say, Type Ib supernovae, in which the He I λ2.0581 μm is weaker than the 1.0830 μm line yet still prominent (Shahbandeh et al. 2022). If the 1 μm feature is associated with He I, it would be very unusual if the 2 μm feature is not seen at all, even if somehow blended by the telluric lines.

Other possibilities include the Mg II λ1.0927 μm, the C I λ1.0693 μm, and the Fe II λ1.0500 μm & λ1.0863 μm. The Mg II λ1.0927 μm is prevalent in the NIR spectra of SNe Ia, but usually disappears within a week after the peak luminosity (Marion et al. 2009), while the 1 μm feature was still visible over a month after the peak in the Keck LRIS spectrum. A stronger Mg II line at 0.9227 μm is not detected either. Also, the problematically high radial velocity of ≈30,000 km/s is not seen in normal SNe Ia, and is over 20% faster than the HVF of Ca II IRT at the same phase.

The C I λ1.0693 μm line from the unburnt carbon is much less frequently seen than the Mg II λ1.0927 μm. Hsiao et al. (2019) presented a sample of five SNe Ia with C I detections, showing the C I feature is strongest for those fainter, fast-declining objects. However, in their sample, the C I feature is always accompanied by the stronger Mg II 1.0927μm line, and is a pre-maximum feature which fades away as the luminosity peaks. The required expansion velocity for C I is ≈22,000 km/s, which is consistent with the HVF of Ca II IRT, but still overwhelmingly faster than the estimated velocity for the sample in Hsiao et al. (2019) (∼10,000-12,000 km/s).

The Fe II features in SNe Ia usually start to develop roughly three weeks after the peak, about the same phase as we obtained our GNIRS spectrum. Two Fe II lines, λ0.9998 μm and λ1.0500 μm, are actually visible on each of the wing of the 1 μm feature. The Fe II λ1.0863 μm line is not yet seen in the GNIRS spectrum. They correspond to an expansion velocity of ≈8,000 km/s, which is consistent with the PVF of the Ca II IRT at the same epoch, and most matches the same two lines for normal SNe Ia (Marion et al. 2009), making the identification more reliable. Obviously, these two Fe II features are wider and shallower than the strong feature between them. We fit the 1 μm feature

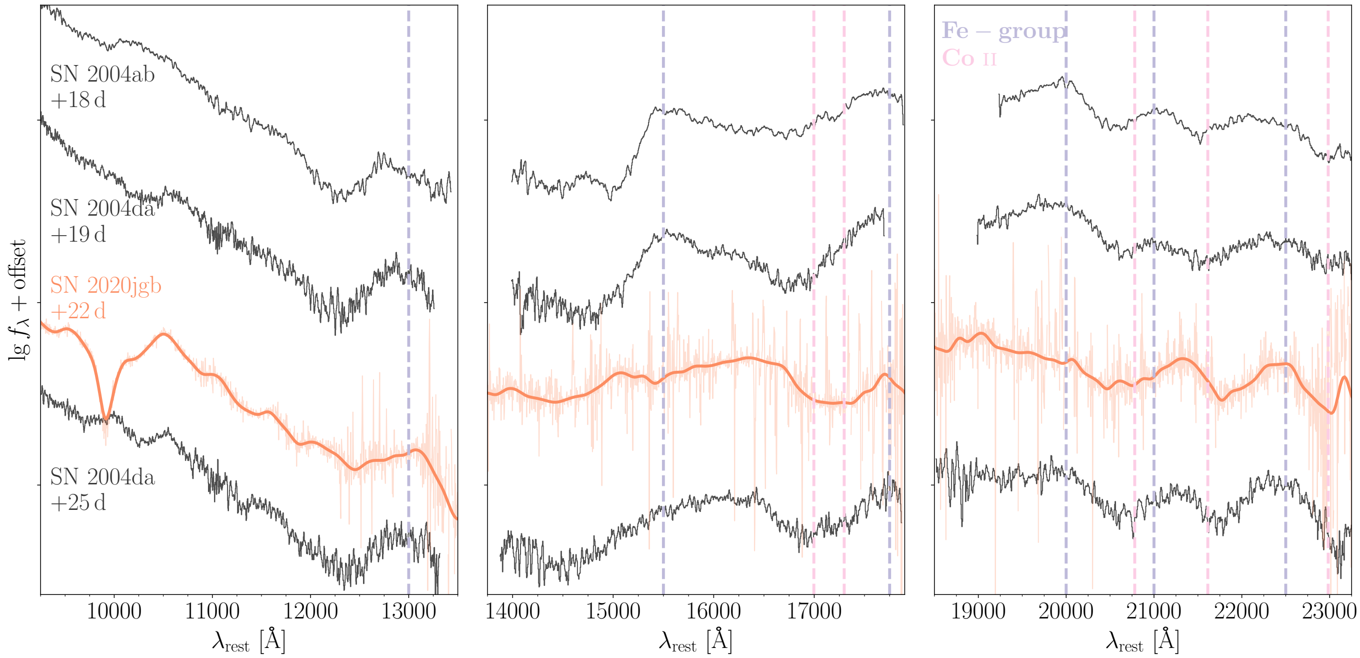

Figure 3. The NIR spectra of SN 2020jgb and two SNe Ia with normal maximum luminosity (SN 2004ab and SN 2004da, Marion et al. 2009), taken about three weeks after the peak. For each spectrum, the continuum at $\gtrsim 1.2\,\mu$m is significantly reshaped by the Fe-group blanketing (emission features, blue vertical lines) and Co II absorption (pink vertical lines).

with three Gaussian profiles. Two of them are set to be the blueshifted Fe II $\lambda 0.9998\,\mu$m and $\lambda 1.0500\,\mu$m, and the other is an uncorrelated Gaussian profile which mainly describes the absorption in the center. We find that the shallower and wider Fe II lines contributes to only ∼40% of the total equivalent width, and the rest ∼60% comes from the central feature, which cannot be accounted for by any Fe II feature at the same velocity. Given the similarity of the Fe-group line blanketing between the GNIRS spectrum with the spectrum of SN 2004da at +25 days, the distribution of Fe-group elements inside each supernova ejecta should be somehow similar, so the central region of the 1 μm feature is not likely to be associated with Fe II.

While the nature of the 1 μm feature remains uncertain, other He-shell double detonation candidates also seem to show similar complexity in this region. In the currently small sample of five candidates, two objects (SN 2016jhr and SN 2019ofm) do not have any available NIR spectra, while the other three all exhibit strong absorption features near 1 μm, though the spectra were obtained at different phases, as shown in Figure 5. The 1 μm feature for SN 2016hnk lies at a longer wavelength than SN 2020jgb, which corresponds to a lower expansion velocity, assuming they all have the same origin. The line velocity assuming a He I $\lambda 1.0830\,\mu$m origin is ≈21,000 km/s, which, just like SN 2020jgb, is about the same as the HVF of the Ca II IRT in the optical spectra. The PVF of the Ca II IRT (≈10,000 km/s) is not significantly slower than that in SN 2020jgb. For SN 2018byg, the velocity of the 1 μm feature with respective to the He I $\lambda 1.0830\,\mu$m is still consistent with the HVF of Ca II IRT. But given its exotic width and lower signal-to-noise ratio, the exact line velocity is hard to determine. It is highly likely to be a mixture of several different lines.

Unfortunately, the NIR spectra for both SN 2016hnk and SN 2018byg do not cover the 2 μm region, thus it is not possible to identify the presence of helium decisively. But if the 1 μm feature of the these objects are of the same origin, they are more likely to be correlated with the high velocity ejecta lying in the outmost region in the supernovae, because at least for SN 2020jgband SN 2016hnk, the difference in their photospheric velocities cannot explain their discrepancy in the line velocities of the 1 μm feature. Then helium is still a promising candidate to cause strong absorption near 1 μm for these sub-luminous He-shell double detonation SNe Ia.

Alternatively, since the NIR spectra for the three objects were all obtained at different epochs, each 1 μm feature can be of completely unrelated origin. This is to be confirmed in a more complete NIR spectral sequence in future He-shell double detonation SNe Ia. Even so, the seemingly ubiquitous 1 μm feature in various phases is possibly a distinctive attribute against normal SNe Ia.

4. HOST GALAXY

5. MODEL COMPARISONS

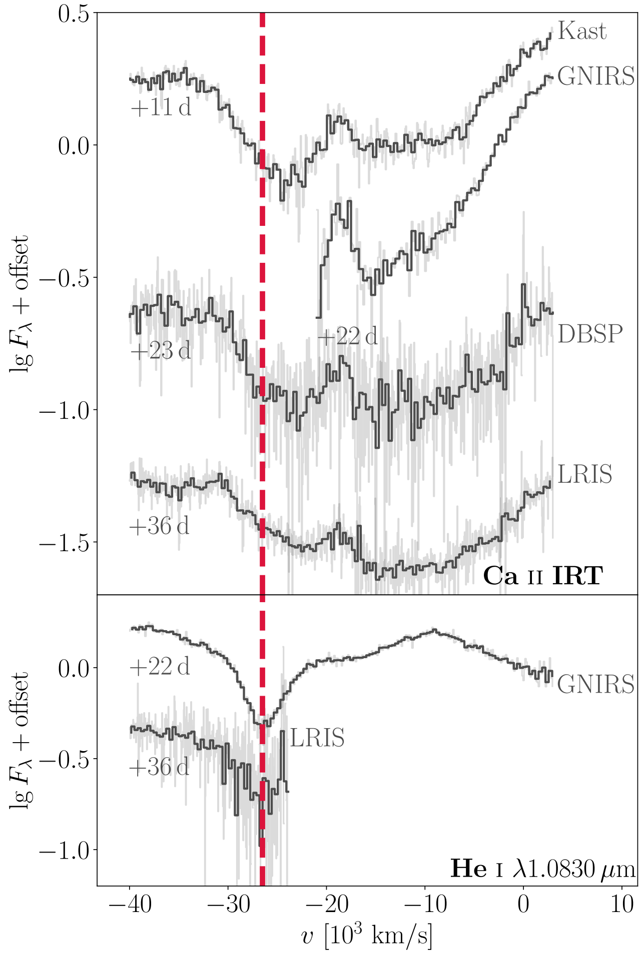

Figure 4. Spectra in the velocity space, comparing the high-velocity component of Ca II IRT and the absorption feature at $\approx$0.99 μm assuming it is associated with He I at 1.0830 μm.

6. DISCUSSION AND CONCLUSION

REFERENCES

Bellm, E. C., Kulkarni, S. R., Graham, M. J., et al. 2019, PASP, 131, 018002, doi: 10.1088/1538-3873/aaecbe

Blagorodnova, N., Neill, J. D., Walters, R., et al. 2018, PASP, 130, 035003, doi: 10.1088/1538-3873/aaa53f

Boyle, A., Sim, S. A., Hachinger, S., & Kerzendorf, W. 2017, A&A, 599, A46, doi: 10.1051/0004-6361/201629712

Brinchmann, J., Charlot, S., White, S. D. M., et al. 2004, MNRAS, 351, 1151, doi: 10.1111/j.1365-2966.2004.07881.x

Bulla, M., Miller, A. A., Yao, Y., et al. 2020, ApJ, 902, 48, doi: 10.3847/1538-4357/abb13c

Cenko, S. B., Fox, D. B., Moon, D.-S., et al. 2006, PASP, 118, 1396, doi: 10.1086/508366

De, K., Kasliwal, M. M., Polin, A., et al. 2019, The Astrophysical Journal, 873, L18, doi: 10.3847/2041-8213/ab0aec

De, K., Kasliwal, M. M., Tzanidakis, A., et al. 2020, The Astrophysical Journal, 905, 58, doi: 10.3847/1538-4357/abb45c

Elias, J. H., Vukobratovich, D., Andrew, J. R., et al. 1998, in Society of Photo-Optical Instrumentation Engineers (SPIE) Conference Series, Vol. 3354, Infrared Astronomical Instrumentation, ed. A. M. Fowler, 555–565, doi: 10.1117/12.317281

Fitzpatrick, E. L. 1999, PASP, 111, 63, doi: 10.1086/316293

Galbany, L., Ashall, C., Höflich, P., et al. 2019, Astronomy & Astrophysics, 630, A76, doi: 10.1051/0004-6361/201935537

Graham, M. J., Kulkarni, S. R., Bellm, E. C., et al. 2019, PASP, 131, 078001, doi: 10.1088/1538-3873/ab006c

Hsiao, E. Y., Phillips, M. M., Marion, G. H., et al. 2019, PASP, 131, 014002, doi: 10.1088/1538-3873/aae961

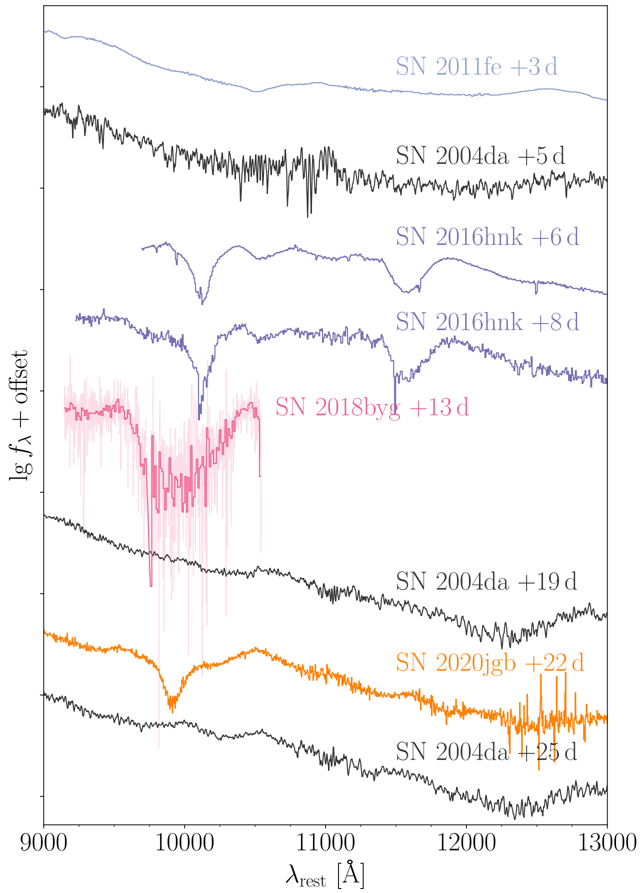

Figure 5. The NIR spectra (9,000 to 13,000 Å) of a few normal SNe Ia (SN 2011fe and SN 2004da) and three He-shell double detonation candidates, which are all subluminous SNe Ia (SN 2016hnk, SN 2018byg, and this source, SN 2020jgb). Spectra for SN 2004da were obtained from Marion et al. (2009), and other spectroscopic data were obtained from the WISEReP repository (Yaron & Gal-Yam 2012).

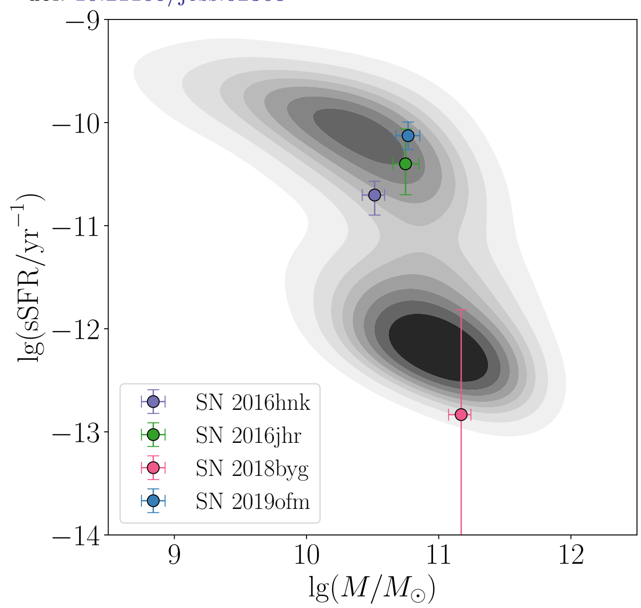

Figure 6. The specific star formation rate (sSFR) and the galactic mass for the host galaxies of He-shell double detonation candidates. The data for the host of SN 2016hnk are taken from Galbany et al. (2019), and for hosts we apply the galaxy parameters from the SDSS MPA-JHU DR8 catalog (Kauffmann et al. 2003; Brinchmann et al. 2004).

Jacobson-Galán, W. V., Polin, A., Foley, R. J., et al. 2020, The Astrophysical Journal, 896, 165, doi: 10.3847/1538-4357/ab94b8

Jiang, J.-a., Doi, M., Maeda, K., et al. 2017, Nature, 550, 80, doi: 10.1038/nature23908

Kauffmann, G., Heckman, T. M., White, S. D. M., et al. 2003, MNRAS, 341, 33, doi: 10.1046/j.1365-8711.2003.06291.x

Marion, G. H., Höflich, P., Gerardy, C. L., et al. 2009, AJ, 138, 727, doi: 10.1088/0004-6256/138/3/727

Oke, J. B., & Gunn, J. E. 1982, PASP, 94, 586, doi: 10.1086/131027

Oke, J. B., Cohen, J. G., Carr, M., et al. 1995, PASP, 107, 375, doi: 10.1086/133562

Prochaska, J. X., Hennawi, J. F., Westfall, K. B., et al. 2020, Journal of Open Source Software, 5, 2308, doi: 10.21105/joss.02308

Prochaska, J. X., Hennawi, J., Cooke, R., et al. 2020, pypeit/PypeIt: Release 1.0.0, v1.0.0, Zenodo, doi: 10.5281/zenodo.3743493

Schlafly, E. F., & Finkbeiner, D. P. 2011, ApJ, 737, 103, doi: 10.1088/0004-637X/737/2/103

Shahbandeh, M., Hsiao, E. Y., Ashall, C., et al. 2022, ApJ, 925, 175, doi: 10.3847/1538-4357/ac4030

Yaron, O., & Gal-Yam, A. 2012, PASP, 124, 668, doi: 10.1086/666656